Hindawi
Applied Bionics and Biomechanics
Volume 2024, Article ID 5870060, 19 pages
https://doi.org/10.1155/2024/5870060

Research Article

Force Tracking Control of Lower Extremity Exoskeleton Based on a New Recurrent Neural Network

Yuxuan Cao,[1] **Jie Chen**,[2] **Li Gao**,[2] **Jiqing Luo**,[2] **Jinyun Pu**,[1] **and Shengli Song**[2]

[1]*Naval University of Engineering, Wuhan 430033, China*
[2]*Army Engineering University, Nanjing 210016, China*

Correspondence should be addressed to Li Gao; gaoli5429@163.com

Received 7 December 2022; Revised 29 November 2023; Accepted 5 December 2023; Published 6 January 2024

Academic Editor: Noé López Perrusquia

The lower extremity exoskeleton can enhance the ability of human limbs, which has been used in many fields. It is difficult to develop a precise force tracking control approach for the exoskeleton because of the dynamics model uncertainty, external disturbances, and unknown human–robot interactive force lied in the system. In this paper, a control method based on a novel recurrent neural network, namely zeroing neural network (ZNN), is proposed to obtain the accurate force tracking. In the framework of ZNN, an adaptive RBF neural network (ARBFNN) is employed to deal with the system uncertainty, and a fixed-time convergence disturbance observer is designed to estimate the external disturbance of the exoskeleton electrohydraulic system. The Lyapunov stability method is utilized to prove the convergence of all the closed-loop signals and the force tracking is guaranteed. The proposed control scheme's (ARBFNN-FDO-ZNN) force tracking performances are presented and contrasted with the exponential reaching law-based sliding mode controller (ERL-SMC). The proposed scheme is superior to ERL-SMC with fast convergence speed and lower tracking error peak. Finally, experimental tests are conducted to verify the efficacy of the proposed controller for solving accurate force tracking control issues.

1. Introduction

When natural disasters such as earthquakes occur in remote mountainous areas, traffic is interrupted, which forces rescuers to enter the disaster area on foot [1]. The rescuers were unable to carry more relief supplies due to physical limitations. By combining the endurance of mechanical device and the intelligence of control system, the lower extremity exoskeleton makes up for human insufficiency in endurance, providing an effective way to accomplish the rescue task [2]. Therefore, the research on lower extremity exoskeleton has scientific significance and great social application requirement in the rescue [3] as well as rehabilitation [4, 5], aid to the disabled [6].

Under load-bearing conditions, each joint of the human lower limbs needs timely active assistance. A lower extremity exoskeleton is presented in Figure 1, where the exoskeleton has seven degree of freedoms (DOFs) for each leg. The exoskeleton directly connects the actuator in parallel to the corresponding joints of the lower limbs. Then, the lower extremity exoskeleton exerts force on the lower limbs through the connection point to achieve active assistance. Timely assistance to active joints is essential to reduce energy consumption of the pilot. As the control of one joint can be easily extended to that of the whole exoskeleton system, for simplicity, only the control problem of a knee joint is considered in this paper.

In rescue scenarios, the payloads carried by the operators are usually quite heavy that high-power supplies are expected. Hydraulic fluid power systems are well-known for their high-power density, many exoskeletons in this direction have been developed, for instance we can refer to the study by Chen et al. [7]. Among them, hydraulic actuators are usually used due to their large values of power/mass ratio [8–10]. However, the dynamics of hydraulic actuators is characteristic with high nonlinearity and time variation, which poses challenges to its corresponding controller design.

Force control is widely used in power augmentation exoskeleton robot due to the fact that its implicitly guarantees a safe and smooth operation for human–robot interaction [11]. Zhang et al. [12] proposed a hierarchical Lyapunov-based

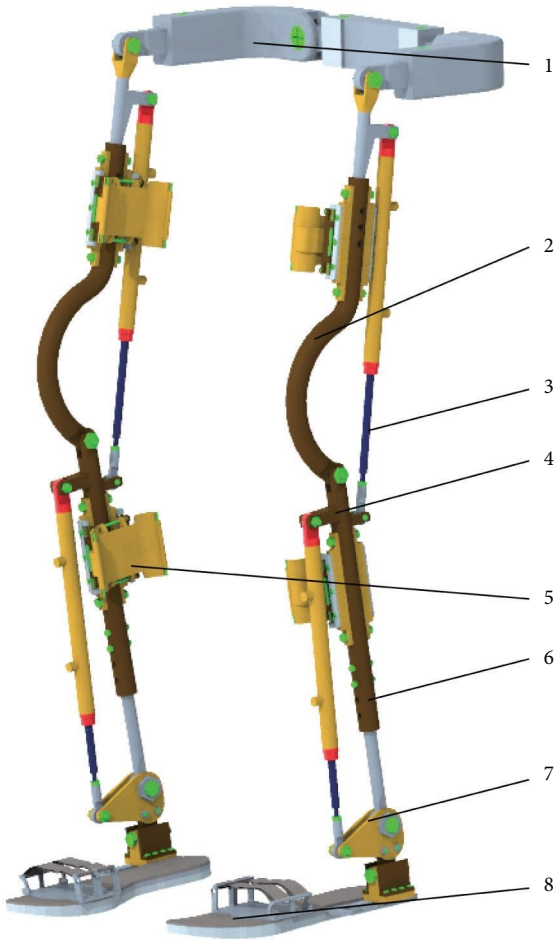

Figure 1: Mechanical structure of the lower extremity exoskeleton: 1-Hip, 2-Thigh, 3-Thigh drive cylinder, 4-Shank, 5-Bound device, 6-Shank drive cylinder, 7-Ankle, and 8-Sole.

cascade adaptive control scheme for lower limb exoskeleton to follow the hydraulic force reference. In view of both cognitive and physical human–robot interaction forces, Lang et al. [13] exhibited a unified framework for scale force control of human-bearing augmentation exoskeleton. Cheng et al. [14] proposed a novel robust adaptive sliding mode control strategy of an electrohydraulic force loading system with consideration of external disturbances and parameter uncertainties. Chen et al. [15] presented an adaptive robust force control algorithm for a lower limb hydraulic exoskeleton to handle the problem of passive joints and holonomic constraints. Song et al. [16] implemented force tracking control of electrohydraulic servo system based on sliding mode control.

However, the force tracking control method mentioned above cannot fully cope with the time-varying challenges of the system. Zhang et al. [17, 18] have formally proposed a novel framework for solving time-varying nonlinear problems, namely zeroing neural network (ZNN). Much related works has been reported in the recent years. Li et al. [19] designed a ZNN model with predefined-time convergence to solve inequality constrained time-invariant quadratic problems. To solve the time-varying super determination problem, Zhang et al. [20] proposed a new variable–parameter convergence differential neural network, which can obtain the least squares solution. An error redefined neural network is proposed in [21] to control the mobile redundant manipulator to perform the tracking task with the redefined error monitoring function taken into account [20]. Zheng et al. [22] and Dai et al. [23] proposed a new controller design based on adaptive multilayer neurodynamics in the ZNN framework, implemented the time-varying trajectory tracking task with external interference and model uncertainty. Besides the predefined-time convergence ZNN [19], and intelligent fuzzy robustness ZNN [24], are also studied to solve the time-varying questions.

In addition, the presence of model uncertainties and the unknown external interference has an impact on the stability of the control system. Neural network methods are wildly utilized to deal with uncertainties in recent years [25]. RBFNN method was proposed to handle the problems of the unknown dynamic model of coordinated dual arms robot and the saturation nonlinearity of the motor [26]. The uncertainties of the robot was approximated by RBFNN [27]. As for the external disturbance, the disturbance observer technology is usually employed in the system for its clear physical significance and simplicity in the engineering implementation [28]. Song et al. [29] proposed a new adaptive neural network control method based on disturbance observer for hydraulic knee exoskeleton. A disturbance observer is designed and integrated into the controller to compensate for external perturbations and equivalent interaction forces acting on the piston rod of the hydraulic actuator.

Based on the analysis above, this paper proposes a new ZNN framework for the exoskeleton with an adaptive RBFNN (ARBFNN) and the fixed-time disturbance observer (FDO) employed to enhance the robustness and force tracking performance of the system. ARBFNN is used to compensate the uncertainty in the model, and the FDO is utilized to estimate the perturbation as well the ARBFNN estimation error.

The rest of this paper is organized into five sections. Section 2 presents the mathematical model of the servo system and the implicit zeroing dynamic of the system. Section 3 designs the control law with disturbance considered, in the meanwhile, the stability and other properties are also analyzed. Section 4 illustrates the simulation results of the proposed method. Section 5 shows the corresponding experimental results. Section 6 concludes the entire paper.

The main contributions of this paper are concluded as followed:

(1) ARBFNN-FDO-ZNN control scheme is proposed for solving exoskeleton force tracking control issues, which builds the bridge among ZNN, observer, and RBFNN.

(2) The problems of model uncertainties, external disturbances, and human–robot interactive force are all considered to enhance the robustness of the system.

(3) The simulation results are carried out for the control scheme and compared with an exponential reaching law-based sliding mode control (ERL-SMC) to track the desired load force to perform its superiority.

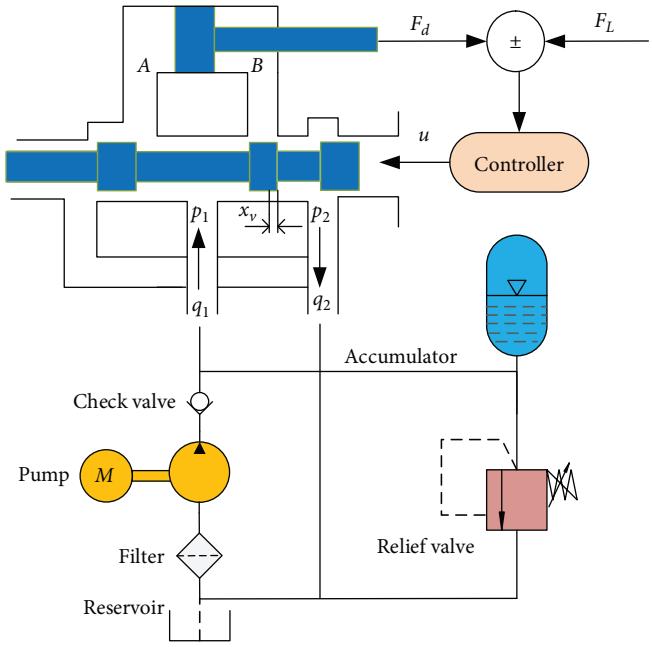

FIGURE 2: Schematic diagram of hydraulic system.

2. Description of the Model

2.1. Mathematical Model. The electrohydraulic system shown in Figure 2 is composed of an oil pimp, a relief valve, a spool valve, a cylinder, an accumulator, etc. The oil pump provides the required high-pressure oil. The accumulator is designed to restore energy during high pressure and supplements the necessary oil to the hydraulic loop during low pressure. The relief valve is introduced to keep the oil pressure stable. A brief introduction to the principle of the hydraulic system is in the following. The piston is pushed by the high-pressure oil from the oil pump. The spool valve position controlled by voltage decides the piston in the cylinder heading left or right. The cylinder displacement reacts accurately as the spool valve displacement varies. In this way, the controller is designed to control the electric current u to gain our ends.

The control objective of the hydraulic exoskeleton is to regulate the voltage of the valve u so that the angle of the exoskeleton joint can track the pilot's trajectory as closely as possible. In the servo system, the voltage u is the control input and the opening degree of the valve is based on it. And the load force F_L is the output. The control voltage is adjusted according to the error between the expected value and the actual value, so that the load force reaches the desired value. Since it is not clear the change in oil temperature and the specific situation of pollution, some simplification is essential. It is assumed that the lower extremity exoskeleton can reach the corresponding angle when the force reaches the desired value. Besides, valves and fluids are considered ideal.

In the following, the model of the hydraulic system is introduced as follows [30]:

$$\begin{cases} \ddot{\varphi} = \frac{1}{J}\left(M\left(F_L + F_f\right) - mgr_o \sin\left(\varphi\right)\right) \\ \dot{F}_L = n_1 x_v - n_2 \dot{x}_c - n_3 F_L + n_4 \\ \dot{x}_v = \frac{1}{\tau}\left(k_s u - x_v\right) \end{cases}, \tag{1}$$

where

$$\begin{aligned} F_f &= \left[F_C + \left(F_S - F_C\right)e^{-(\dot{x}_c/v_s)^2}\right]sgn(\dot{x}_c) + \mu\dot{x}_c \\ n_1 &= \frac{\beta(A_1+A_2)K_q}{V_0} \\ n_2 &= \frac{\beta(A_1+A_2)^2}{2V_0} \\ n_3 &= \frac{\beta(2K_c+2C_{in}+C_{ex})}{V_0}. \end{aligned}$$

The nomenclature appearing in Formula (1) is listed in Nomenclature Section.

2.2. Force Tracking Dynamic. In this paper, we explore force tracking control. Therefore, the load force is the subsystem. Let x be $[F_L x_v]^T$, and a subsystem Formula (2) is defined as follows:

$$F(x,u) = \begin{bmatrix} n_1 x_v - n_2 \dot{x}_c - n_3 F_L + n_4 \\ \frac{1}{\tau}k_s u - \frac{1}{\tau}x_v \end{bmatrix}. \tag{2}$$

Model (2) can be transformed into the following forms:

$$\begin{cases} \dot{x}(t) = Ax + G(x,u) \\ y(t) = Cx(t) \end{cases}, \tag{3}$$

where A is selected such that A is Hurwitz stable and the pair (C, A) is observable.

An error function is given as $e(t) = Ax + G(x,u) - \dot{x}_d(t)$. The evolution of the error function is defined as $\dot{e}(t) = -\gamma e(t)$, where $\gamma > 0$ is the design parameter. Thus, a conventional ZNN model is completed.

$$A\dot{x}(t) + \dot{G}(x,u) - \ddot{x}_d(t) = -\gamma[Ax + G(x,u) - \dot{x}_d(t)]. \tag{4}$$

3. Controller Design

However, the force tracking model is ideal. Actually, disturbance and errors often lie in the model implementation, such as differentiation error. Thus, the robustness of this subsystem should be taken into account.

In the noise-free case, the conventional ZNN converges to the desired result globally and exponentially (Theorem 1). Therefore, the polluted design formula of ZNN is explored in this paper. Besides, Figure 2 indicates the piston displacement x_c is crucial to the whole hydraulic system and easily affected by the external factors. In this section, the control input u is designed with polluted ZNN design formula and the differentiation error of x_c considered. Besides, the system

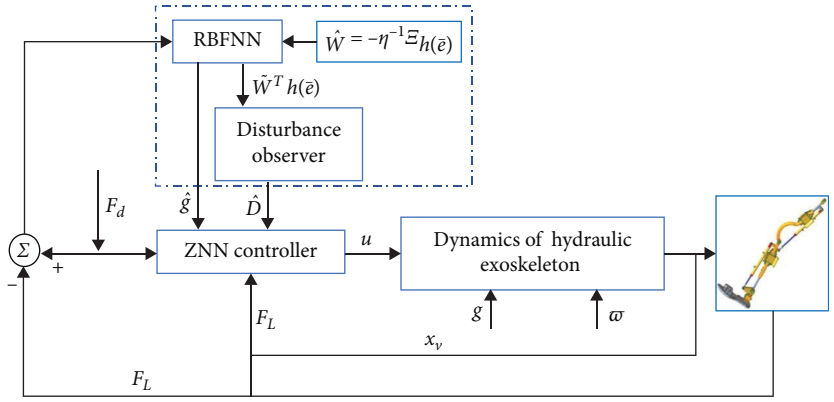

Figure 3: Control diagram of hydraulic exoskeleton.

uncertainty and external disturbances are inevitable in practical. The structure of force tracking system is shown in Figure 3.

3.1. Polluted ZNN Controller Design. u is implicited in Formula (4). For convenience, we perform the explicit conversion. The mathematical model introduced can be regarded as a one-dimension matrix. The selection of different variables has a direct effect on the derived control law. We define $x_1 = F_L$, $x_2 = \dot{F}_L$, and $x_3 = x_v$. Then, the system Formula (1) is transformed into the following form with model uncertainties, external disturbances, and human–robot interaction force considered [5] as follows:

$$\begin{cases} \dot{x}_1 = x_2 \\ \dot{x}_2 = n_1\dot{x}_3 - n_2\left(\ddot{x}_c + \Delta d^{(2)}\right) - n_3 x_2 + g_1 + \varpi_1 \\ \dot{x}_3 = \dfrac{1}{\tau}(k_s u - x_3) + g_2 + \varpi_2 \\ y = x_1 \end{cases}, \tag{5}$$

where $\Delta d^{(n)}$ $(n = 1, 2\ldots)$ denotes the corresponding differentiation error of x_c, g_1, and g_2 denote the system uncertainty; ϖ_1 and ϖ_2 denote the unknown human–robot interactive force and the external disturbance, respectively.

Remark 1. During the movement, human–robot interaction force is inevitable in the system. Mathematically, the interactive force ϖ_1 can be depicted as follows:

$$\varpi_1 = k_p(F_L - F_d) + k_d\left(\dot{F}_L - \dot{F}_d\right), \tag{6}$$

where parameters k_p and k_d are constant values that amplify the differences between machine and human, F_d is the desired force.

Assumption 1. *For system Formula (5), there are bounded positive constants ϖ_1, ϖ_2, $\overline{g}_1$, and $\overline{g}_2$ that satisfy the inequality $|\varpi_1| \le \overline{\varpi}_1$, $|\varpi_2| \le \overline{\varpi}_2$, $|g_1| \le \overline{g}_1$, and $|g_2| \le \overline{g}_2$.*

First step: according to the design process of ZNN, the first Zhang function (ZF) is constructed and applied as follows:

$$e_1 = x_1 - x_d, \tag{7}$$

where x_d denotes the desired force F_d.

$$\dot{e}_i = \frac{d\dot{e}_i}{dt} = -\gamma\phi(e_i) + \Delta f_i, i = 1, 2\ldots, \tag{8}$$

where the design parameter $\gamma > 0$ scales the convergence rate and Δf_i represents the bounded noise with each entry $\Delta f_i \le f$. Different values of γ puts various influences on the tracking performance as well Δf.

Within the hydraulic system that can afford, the higher γ is set, the better the tracking performance is exhibited. $\phi(\cdot)$ is an activation function. In theory, an arbitrary odd monotonically increasing activation functions can be used for the ZF construction. Zhang et al. have discussed the different activation functions. Considering the simplicity of the controller, the linear function $\phi(e_i) = e_i$ is selected. Then we can obtain

$$\dot{e}_1 = \dot{x}_1 - \dot{x}_d. \tag{9}$$

The design Formula (8) is applied, and we get

$$\dot{x}_1 - \dot{x}_d = -\gamma(x_1 - x_d) + \Delta f_1. \tag{10}$$

Since $\dot{x}_1 = x_2$, we have

$$x_2 + \gamma(x_1 - x_d) - \dot{x}_d - \Delta f_1 = 0. \tag{11}$$

Second step: in general, e_1 and $\dot{e}_1$ does not always equal zero when $t = 0$. Besides, no explicit expression of u is contained in Formula (11), the further consideration of the controller design is necessary. Then the second ZF is constructed as follows:

$$e_2 = x_2 + \gamma(x_1 - x_d) - \dot{x}_d - \Delta f_1. \tag{12}$$

ZNN design Formula (8) is applied again. Then, we get

$$x_2 + \gamma x_1 - \ddot{x}_d - \gamma \dot{x}_d = -\gamma(x_2 - \gamma x_1 - \gamma x_d - \dot{x}_d - \Delta f_1) + \Delta f_2. \tag{13}$$

Then,

$$\dot{x}_2 = n_1 \dot{x}_3 - n_2\left(\ddot{x}_c + \Delta d^{(2)}\right) - n_3 x_2 + g_1 + \varpi_1. \tag{14}$$

Substituting it into the equation above, the control law for the hydraulic system Formula (5) can be depicted below

$$\begin{aligned} u = \frac{\tau}{n_1 k_s}\Big[& -\gamma^2 x_1 + (n_3 - 2\gamma)x_2 + \gamma^2 x_d \\ & + 2\gamma \dot{x}_d + \ddot{x}_d + n_2 \dddot{x}_c + \frac{n_1 x_3}{\tau}\Big] + g + \varpi, \end{aligned} \tag{15}$$

where $g = \frac{\tau}{n_1 k_s}(\gamma \Delta f_1 + \Delta f_2 + n_2 d^{(2)} - g_1 - n_1 g_2)$ can be regarded as the internal disturbance in the system, $\varpi = \frac{\tau}{n_1 k_s}(\varpi_1 + n_1 \varpi_2)$ is considered as the lumped external disturbance.

Theorem 1. *(Global and exponential convergence without noise) Given the necessary parameters, if linear activation and design formula are used, the solution error $e_1 = x_1 - x_d$ converges to zero globally and exponentially at any randomly generated initial state $F_L(0)$.*

Proof. ZNN design formula is as $\dot{e}_1 = -\gamma \phi(e_1)$. Then, a Lyapunov function candidate for the system is defined as follows: □

$$V_1 = \frac{e_1^2}{2}. \tag{16}$$

It is obvious that the Lyapunov function is positive-definite, because for any $\dot{e}_1 \neq 0$ and $V_1 > 0$. Besides, $V_1 = 0$ exists only for $\dot{e}_1 = 0$. Next, its time derivative can be obtained below. Since the linear activation function $\phi(e_i) = e_i$ is utilized, we have,

$$V_1 = -\gamma e_1 \phi(e_1) = -\gamma e_1^2 \leq 0, \tag{17}$$

which guarantees the negative-definite of $\dot{V}_1$. The equation sign makes sense if and only if the condition that $e_1 = 0$ is satisfied. Based on Lyapunov theory, e_1 globally converges to zero. In view of this, the proof of global convergence is thus completed.

Next, we verify the exponential convergence. In consideration of ZNN error function, its analytic solution can be obtained as follows:

$$e_1 = e_1(F_L(0)) \exp(-\gamma t). \tag{18}$$

Evidently, with $t \to \infty$, the tracking error converges to zero exponentially with convergence rate γ, and the proof is done. It is worth pointing out that, it follows from Formula (18) that the larger γ is used, the faster convergence rate is obtained.

Theorem 2. *(The error bound with noise) The polluted ZNN design Formula (7) is given. Whether the constant or time-varying noise, the absolute steady-state error of the system satisfies the following equality:*

$$\lim_{t \to \infty} |e_1| < \frac{1}{\gamma} f. \tag{19}$$

Proof. A Lyapunov function candidate $V_2 = \frac{1}{2}|e_1|^2 \geq 0$ is considered for the system Formula (5). Taking the derivation of it, we can obtain □

$$\begin{aligned} \dot{V}_2 &= |e_1| sgn(e_1)(-\gamma |e_1| sgn(e_1) + \Delta f_1) \\ &= -\gamma\left(|e_1| sgn(e_1) - \frac{1}{2\gamma}\Delta f_1\right)^2 + \frac{1}{4\gamma}\Delta f_1^2, \end{aligned} \tag{20}$$

where $sgn(\cdot)$ is the symbolic function. Besides, the following inequality yields

$$\left||e_1| sgn(e_1) - \frac{1}{2\gamma}\Delta f_1\right| \geq |e_1| - \frac{1}{2\gamma} f. \tag{21}$$

According to the results above, Formula (20) falls into the following two situations.

(1) If $e_1 > \frac{f}{\gamma}$, then $\dot{V}_2 \leq 0$, indicating the value of V_2 decrease over time. Such that $V_2 \to 0$ with $t \to +\infty$. Therefore, $|e_1|$ will return to its upper bound $\frac{f}{\gamma}$.

(2) If $e_1 < \frac{f}{\gamma}$, then the sign of $\dot{V}_2$ is uncertain. If $\dot{V}_2 \leq 0$, the tracking error decreases or remains unchanged. Even though $\dot{V}_2 \geq 0$, the tracking error will increase with time. The tracking error does not exceed its upper bound $\frac{f}{\gamma}$. Once the tracking error exceeds the upper bound, it falls into the first situation. Then we can readily obtain $\lim_{t \to +\infty} |e_1| < \frac{f}{\gamma}$.

The proof is thus completed.

3.2. Adaptive RBFNN and Fixed-Time Convergence Disturbance Observer Design. Clearly, the control law cannot achieve for the disturbance in the system.

First, the internal disturbance is approximated. It has been noted that a three-layer RBFNN with only one single-hidden layer is sufficient to approximate any degree of nonlinear system [31]. Then, RBFNN is introduced for estimating the

unknown part of u. Δf_i is bounded as well the system uncertainty and it can be substituted by the corresponding upper bound, which is conservative. Therefore, RBFNN is utilized to approximate g to enhance the performance of the controller.

Lemma 1. *RBFNN can be utilized to approximate any continuous function $F(x)$: $\mathbb{R}^m \to \mathbb{R}$ arbitrarily [31].*

$$F(x) = \widehat{W}^T h(x) + \varepsilon, \tag{22}$$

where $\widehat{W}$ is the weight matrix, $x = [x_1, x_2, \ldots x_n]^T$ is the input vector, $h(x) = [h_1(x), h_2(x), \ldots, h_j(x)]^T$ is the radius basis function, ε is the approximation error, j is the number of neuron nodes. The ideal weight matrix is defined as follows:

$$W^* = \underset{\widehat{W} \in \Omega_F}{\operatorname{argmin}} \left[\sup_{x \in \Omega_x} \left\| \widehat{W}^T h(x) - F(x) \right\| \right], \tag{23}$$

where $\Omega_F = \{\widehat{W} \mid \|\widehat{W}\| \le M\}$ is the effective estimation domain, M is the design parameter, and $\Omega_x \in \mathbb{R}^m$ is the feasible region for states vector, respectively. $h_i(x)$ is defined as follows:

$$h_i(x) = \exp\left(-\frac{\|x - c\|^2}{2b^2} \right), \tag{24}$$

where c is the coordinate vector of the basis function center point, and b is the width of the basis function, $i = [1, 2, 3\ldots, j]$.

According to Lemma 1, RBFNN is utilized to estimate the unknown function g as follows:

$$g = W^{*T} h(\bar{e}) + \varepsilon^*, \tag{25}$$

where W^*, $\bar{e} = [x_1 \quad x_2 \quad e_1 \quad \dot{e}_1]$ are the perfect output weights vector and the input of RBFNN, respectively, ε^* is the neural network functional approximation error that is bounded, $|\varepsilon^*| \le \varepsilon_0$, ε_0 is a small positive constant and in principle can be arbitrarily small by adjusting RBFNN, $h(\cdot)$ is RBFNN activation function. The output can be approximated by

$$\widehat{g} = \widehat{W}^T h(\bar{e}), \tag{26}$$

where $\widehat{W}^T$ is the actual weight matrix.

Next, we design the disturbance observer and the adaptive law for RBFNN weight matrix. The structure of ARBFNN is given in Figure 4.

The approximation error of RBFNN ε^* and the external disturbance ϖ consist of the compound disturbance. We let $D = \varepsilon^* + \varpi$. Considering Assumption 1 and Lemma 1, the compound disturbance is bounded, that is to say, there is a positive constant which satisfies the inequality $|D| \le \overline{D}$.

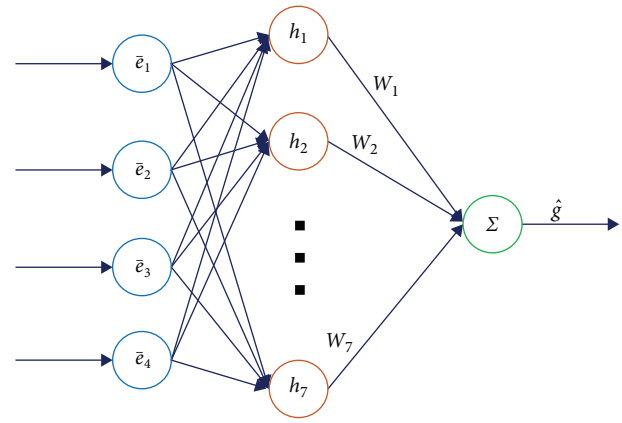

Figure 4: ARBFNN structure.

Because D is unknown, the disturbance observer is designed to approximate this term.

First, define a variable $\Xi = x_2 - z$ where z is the auxiliary variable. And the derivate of z is shown as follows:

$$\begin{aligned} \dot{z} = &\left(n_1 \dot{x}_3 - n_3 x_2 - n_2 \ddot{x}_c + \widehat{W}^T h(\bar{e}) \right) \\ &+ L\left(\Xi + \Xi^r + \Xi^{\frac{1}{r}} + \text{sigmoid}(\Xi) \right), \end{aligned} \tag{27}$$

where $r \in (0, 1)$ is a positive constant, L is the gain parameter. Based on Formula (27) and Formula (5), we have,

$$\dot{\Xi} = \dot{x}_2 - \dot{z} = D - L\left(\Xi + \Xi^r + \Xi^{\frac{1}{r}} + \text{sigmoid}(\Xi) \right) - \widetilde{W} h(\bar{e}), \tag{28}$$

where $\tilde{W}^T = \widehat{W}^T - W^{*T}$. The specific form of disturbance observer is given as follows:

$$\widehat{D} = L\left(\Xi + \Xi^r + \Xi^{\frac{1}{r}} + \text{sigmoid}(\Xi) \right) + \widetilde{W} h(\bar{e}). \tag{29}$$

The control law for u is given as follows:

$$\begin{aligned} u = \frac{\tau}{n_1 k_s} [&- \gamma^2 x_1 + (n_3 - 2\gamma) x_2 + \gamma^2 x_d + 2\gamma \dot{x}_d + \ddot{x}_d + n_2 \ddot{x}_c \\ &+ \frac{n_1 x_3}{\tau} + \widehat{W}^T h(\bar{e}) + \widehat{D}]. \end{aligned} \tag{30}$$

Further, the observer error is defined as follows:

$$\begin{aligned} \widetilde{D} = D - \widehat{D} = &-L\left(\Xi + \Xi^r + \Xi^{\frac{1}{r}} + \text{sigmoid}(\Xi) \right) \\ &- \widetilde{W} h(\bar{e}) + D = \dot{\Xi} \end{aligned} \tag{31}$$

Lemma 2. *If a continuous radial bounded function $V: \mathbb{R}^n \to \mathbb{R}_+ \cup \{0\}$ satisfies [32]:*

(1) $V(x) = 0 \Leftrightarrow x = 0$
(2) *For any* $x(t)$ *satisfying the inequality*

$$\dot{V}(x) \leq -k_1 V^a(x) - k_2 V^{a_1}(x) + \vartheta, \tag{32}$$

then the system is globally stable and converges in fixed time, where $k_1, k_2 > 0$, $0 < a < 1$, $a_1 > 1$, *and* $\vartheta \in (0, +\infty)$. *The convergence time T satisfies the inequality as follows:*

$$T \leq T_{\max} := \frac{1}{k_1 \psi(1-a)} \frac{1}{k_2 \psi(a_1 - 1)}, \tag{33}$$

where ψ *is a constant with* $0 < \psi < 1$

Theorem 3. *(Fixed-time stable disturbance observer) If the disturbance observer Formula (29) is adopted, the compound disturbance D could be estimated in fixed time T, and the disturbance error is 0.*

Proof. From Formula (31), it is obtained that if $\dot{\Xi}$ converges to zero, its corresponding derivative converges to 0 as well $\tilde{D}$. □

A Lyapunov candidate is chosen as follows:

$$V_3 = 0.5\Xi^2 + 0.5\eta \widetilde{W}^T \widetilde{W}. \tag{34}$$

The derivate of V_3 is as follows:

$$\begin{aligned}
\dot{V}_3 &= \Xi\dot{\Xi} + \eta \widetilde{W}^T \dot{\widetilde{W}} \\
&= \Xi\left(-L\left(\Xi + \Xi^r + \Xi^{\frac{1}{r}} + \text{sigmoid}(\Xi)\right) - \widetilde{W}^T h(\bar{e}) + D\right) \\
&\quad -\eta \widetilde{W}^T \dot{\widehat{W}} \\
&\leq -L\Xi^{r+1} - L\Xi^{\frac{1}{r}+1} + \left|\overline{D}\Xi - L\Xi\text{sigmoid}(\Xi)\right| \\
&\quad \underbrace{-\widetilde{W}^T\left(\Xi h(\bar{e}) + \eta\dot{\widehat{W}}_1\right)}_{set=0}.
\end{aligned} \tag{35}$$

The adaptive law for RBFNN is given as follows:

$$\dot{\widehat{W}} = -\eta^{-1}\Xi h(\bar{e}), \tag{36}$$

where $\eta > 0$ is the design parameter. Such that,

$$\begin{aligned}
\dot{V}_3 \leq & -L\left(2V_3 - \eta\widetilde{W}^T\widetilde{W}\right)^{\frac{(r+1)}{2}} - L\left(2V_3 - \eta\widetilde{W}^T\widetilde{W}\right)^{\frac{(r+1)}{2r}} \\
& + \left|\overline{D}\Xi - L\Xi\text{sigmoid}(\Xi)\right|.
\end{aligned} \tag{37}$$

For the analysis, r is taken as 1/3 in the paper. Notice, $\tilde{W}^T\tilde{W} \geq 0$, $\eta > 0$ and $2V_3 - \eta\tilde{W}^T\tilde{W} \geq 0$. Then, Formula (37) is rewritten as follows:

$$\begin{aligned}
\dot{V}_3 &\leq -L\left(2V_3 - \eta\widetilde{W}^T\widetilde{W}\right)^2 - L\left(2V_3 - \eta\widetilde{W}^T\widetilde{W}\right)^{\frac{2}{3}} \\
&\quad + \left|\overline{D}\Xi - L\Xi\text{sigmoid}(\Xi)\right| \\
&\leq -4LV_3^2 - L\left(2V_3 - \eta\widetilde{W}^T\widetilde{W}\right)^{\frac{2}{3}} \\
&\quad + \left|\overline{D}\Xi - L\Xi\text{sigmoid}(\Xi)\right| + 4L\eta V_3 \widetilde{W}^T\widetilde{W} - L\left(\eta\widetilde{W}^T\widetilde{W}\right)^2.
\end{aligned} \tag{38}$$

Clearly, $4L\eta V_3\tilde{W}^T\tilde{W} - L(\eta\tilde{W}^T\tilde{W})^2 \geq 0$. Besides, for the term $-L(2V_3 - \eta\tilde{W}^T\tilde{W})^{\frac{2}{3}}$, we have the following analysis.

We construct a continuous function $f(x)$.

$$f(x) = -Lx^{\frac{2}{3}}, x \in [0, +\infty). \tag{39}$$

Based on Lagrange mean value theorem, there exists a positive constant α satisfying as follows:

$$f'(\alpha) = \frac{f(2V_3) - f\left(2V_3 - \eta\widetilde{W}^T\widetilde{W}\right)}{\eta\widetilde{W}^T\widetilde{W}} \leq 0, \tag{40}$$

where $\alpha \in (2V_3 - \eta\tilde{W}^T\tilde{W}, 2V_3)$.

Then, $-L(2V_3 - \eta\tilde{W}^T\tilde{W})^{\frac{2}{3}}$ can be expressed in the following form:

$$-L\left(2V_3 - \eta\widetilde{W}^T\widetilde{W}\right)^{\frac{2}{3}} = -2^{\frac{2}{3}}LV_3^{\frac{2}{3}} - f'(\alpha)\eta\widetilde{W}^T\widetilde{W}. \tag{41}$$

Formula (38) is reformulated as follows:

$$\dot{V}_3 \leq -4LV_3^2 - LV_3^{\frac{2}{3}} + \vartheta, \tag{42}$$

where $\vartheta = -f'(\alpha)\eta\tilde{W}^T\tilde{W} + \left|\overline{D}\Xi - L\Xi\text{sigmoid}(\Xi)\right| + 4L\eta V_3\tilde{W}^T\tilde{W} - L(\eta\tilde{W}^T\tilde{W})^2 \geq 0$. From Lemma 2, we can obtain the following inequality:

$$T \leq T_{\max} := \frac{1}{k_1\psi(1-a)} \frac{1}{k_2\psi(a_1 - 1)}, \tag{43}$$

where $k_1 = 2^{\frac{2}{3}}L$, $k_2 = 4L$, $a = \frac{2}{3}$, $a_1 = 2$, respectively.

The proof is completed.

Theorem 4. *(Robustness analysis) Considering the system Formula (5) with uncertainties and external disturbances, if RBFNN Formula (26), its adaptive law Formula (36), disturbance observer Formula (29) are employed, the system tracking error* e_1, e_2 *are fixed time stable.*

Proof. A Lyapunov function candidate is selected as follows: □

$$V_4 = V_1 + V_3 + 0.5e_2^2. \tag{44}$$

The derivative of V_4 is described by

$$\begin{aligned}\dot{V}_4 &= 0.5e_1\dot{e}_1 + 0.5e_2\dot{e}_2 + \dot{V}_3 \\ &= -\gamma(e_1^2 + e_2^2) + \dot{V}_3 \\ &\leq \dot{V}_3 \leq -4LV_3^2 - 2^{\frac{2}{3}}LV_3^{\frac{2}{3}} + \vartheta.\end{aligned} \tag{45}$$

We construct a continuous function

$$f_1(x) = -4Lx^2 - 2^{\frac{2}{3}}Lx^{\frac{2}{3}}, x \in [0, +\infty). \tag{46}$$

It is common to find that $f_1(x)$ is a monotonically decreasing function. Since $V_4 \geq V_3$, we have,

$$f_1(V_3) = f_1(V_4) + \rho, \tag{47}$$

where $\rho \geq 0$.

Then, Formula (45) is converted to

$$\begin{aligned}\dot{V}_4 &\leq -4LV_3^2 - 2^{\frac{2}{3}}LV_3^{\frac{2}{3}} + \vartheta \\ &= -4LV_4^2 - 2^{\frac{2}{3}}LV_4^{\frac{2}{3}} + \vartheta + \rho.\end{aligned} \tag{48}$$

Therefore, the tracking error e_1, e_2 are fixed time stable. From Lemma 2, the convergence time $T1$ satisfies as follows:

$$T \leq T_{\max} := \frac{1}{k_1\psi(1-a)}\frac{1}{k_2\psi(a_1 - 1)}, \tag{49}$$

where $k_1 = 2^{\frac{2}{3}}L, k_2 = 4L, a = \frac{2}{3}, a_1 = 2$, respectively.

4. Simulation Studies

The simulation is presented in this section to demonstrate the effectiveness and superiority of the proposed control scheme. It has been discussed in Section 2 that the desired force is determined by the angle joint and the actuator displacement. There is a functional relationship between joint angle φ and load force F_L. Considering the simplicity of the system, the desired load force is chosen as the reference quantity.

To avoid adverse effects caused by simulation parameters, the main parameters are selected as shown in Table 1. The considered disturbances in this paper are shown in Table 2, including four different common disturbances [33]. In this work, the ERL-SMC controller is used as a contrast control strategy. The corresponding controller without considering disturbances is given as follows:

Table 1: The main parameters of the electrohydraulic servo system.

Parameters	Units	Value
m	kg	50
β	s^{-1}	$1.517e^9$
μ	Ns/m	10,000
p_s	MPa	8
τ	s	0.0035
F_C	N	4
$2C_{in} + C_{ex}$	–	$3e^{-14}$
K_c	m^3 s/Pa	$2.0e^{-11}$
K_q	m^3 s · A	$18.2e^{-3}$
k_s	m/MPa	1.54
A_1	m^2	$3.25e^{-4}$
A_2	m^2	$2.1e^{-4}$

Table 2: The disturbances forms.

No.	Disturbance forms	Expression
1	Constant form	1
2	Random form	rand(1)
3	Sine form	$\sin(2\pi t)$
4	Exponential-decay form	$\exp(-t)$

$$\begin{aligned}u_{\text{ERL-SMC}} = \frac{\tau}{n_1 k_s}[&\ddot{x}_d + n_2\ddot{x}_c + n_3 x_2 + \delta(\dot{x}_d - x_2) \\ &+ ks + \zeta \tanh(s)],\end{aligned} \tag{50}$$

where s is the sliding function, δ, ζ, and k are positive constants, respectively. Similar to γ, k is used to adjust the convergence rate.

The simulation is repeated to observe the effects of the controller with various load forces and frequencies. We set the desired force as $F_d = 200 \times \sin(4\pi t)$ and $F_d = 200 \times \sin(20\pi t)$, respectively. The external disturbance and interactive force related terms are given as $\varpi = \sin(2\pi t) + 1 + \exp(-0.1t)$ and $g = 0.05x_1 + 10^{-3}x_2$. The control law (30), ARBFNN (26), its adaptive law (36), and FDO (29) are employed. ZNN design parameter γ is set to be 100, 200, and 300, respectively. The structure of ARBFNN is 4-7-1. ARBFNN parameters are given as $c_i = 10^3[-2.5, -1.7, -0.9, 0, 0.9, 1.7, 2.5]$, $b = 10^3$, and $\eta = 0.005$. The disturbance observer parameters L, r are set to be 1 and 1/3, respectively. The initial condition is set to be $F_L(0) = 0$. As for ERL-SMC controller, the corresponding parameters are selected as $\delta = 15$, $\zeta = 10$, and $k = 100, 200, 300$. The sampling period is selected as 0.001 s. All simulation experiments are conducted on MATLAB/Simulink R2020b. The ode 3 solver is selected.

The blue dot dash line in Figure 5(a) shows that the proposed controller can track the desired force quickly. As presented in Figure 5(c) blue solid line, the maximum force tracking error for the proposed is 9.24 N. After 0.113 s, the tracking error reaches stable state. From Theorem 1, the

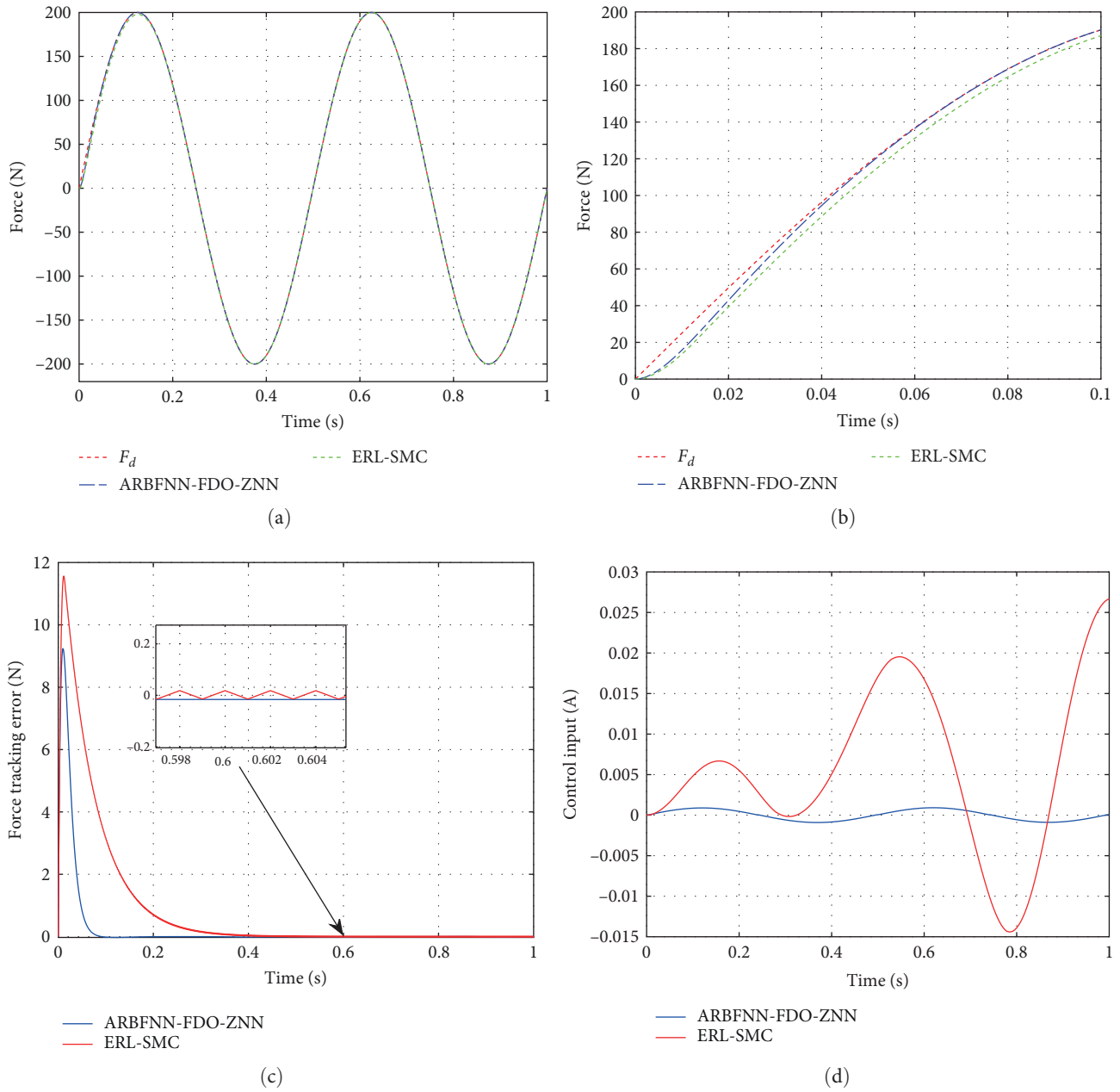

FIGURE 5: The simulation comparison results with $F_d = 200\sin(4\pi t)$, $\gamma = 100, k = 100$. (a) Represents the overall simulation results, (b) represents the partial enlargement of (a), (c) is the tracking error, and (d) reveals the control input signal.

maximum tracking error can be reduced by adjusting the design parameter γ. Then, γ is set to be 200 in Figure 6. Compared to Figure 5(c), the maximum tracking error of the proposed scheme reduces to 4.62 N in Figure 6(c), reduced by 50% and the convergence time drops from 0.113 to 0.47 s. Evidently, the increased γ leads to the diminishing peak value and convergence time.

Furthermore, frequency can affect performance of the proposed controller. The blue dot dash line in Figures 6(c) and 7(c) indicates the increased frequency leads to a significant increase in maximum tracking error. Accordingly, the design parameter γ can be adjusted to enhance the control quality.

To demonstrate the superiority of the ARBFNN-FDO-ZNN framework, we compare it with ERL-SMC in terms of maximum tracking error and convergence time. The key parameters γ and k are kept same for fair comparison. The comparative results are listed in Tables 3 and 4. Besides, partial enlargements (red solid line) in Figures 5(c)–8(c) illustrate the stable tracking error of ERL-SMC still oscillates with time. On the contrary, the tracking error of ARBFNN-FDO-ZNN is relatively smooth. There is no doubt the proposed control scheme performs its excellence. The evolution of the adaptation weights $\widehat{W}$ by ARBFNN are shown in Figure 9.

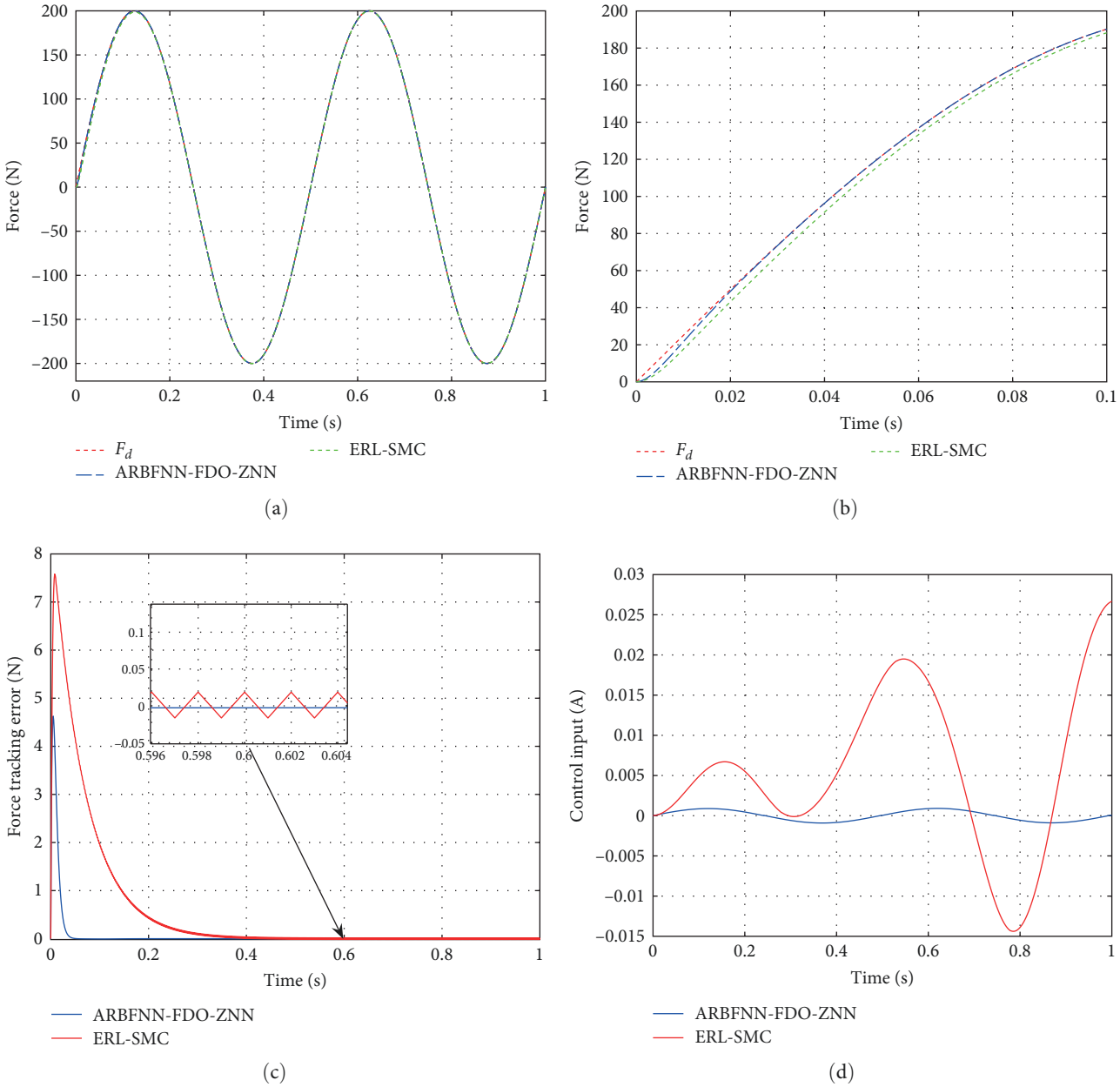

FIGURE 6: The simulation comparison results with $F_d = 200\sin(4\pi t)$, $\gamma = 200$, and $k = 200$. (a) Represents the overall simulation results, (b) represents the partial enlargement of (a), (c) is the tracking error, and (d) reveals the control input signal.

5. Experimental Results

The effectiveness of the controller is further validated in experiments on the robot servo system. The block diagram is depicted in Figure 10. The proper hydraulic cylinder and servo valve are selected to meet the specific requirements. The computer disposition is Intel Core I7/2.8 G Hz, 8G memory, 250 G solid state disk with a 32-bit A/D converter, a 32-bit D/A converter, and an amplifier. The desired force signal is generated by the computer. The controller is adopted to control the servo system. The experimental results are demonstrated in Figures 11–14.

Comparing Figure 11(c) with Figure 8(c), the maximum tracking error of experimental results is 1.38 N higher than that of simulation results, a increase of 14.9%. Considering the given reference is $F_d = 200\sin(4\pi t)$, the maximum tracking error of the algorithm is within the allowable range of engineering applications. To observe the influence of the design parameter, we increase the design parameters from 100 in Figure 11 to 200 in Figure 12. Correspondingly, it is found that the peak value is reduced from 10.62 in to 5.24 N.

Besides, we have investigated the effect of frequency variation on the control effect. All else being equal, the higher frequency has the negative impact on the experimental tracking performance (Figures 12 and 13), which is consistent with the simulation results. To resist the negative effects of frequency variations and enhance the control performance shown in Figure 13, we have increased the design parameter

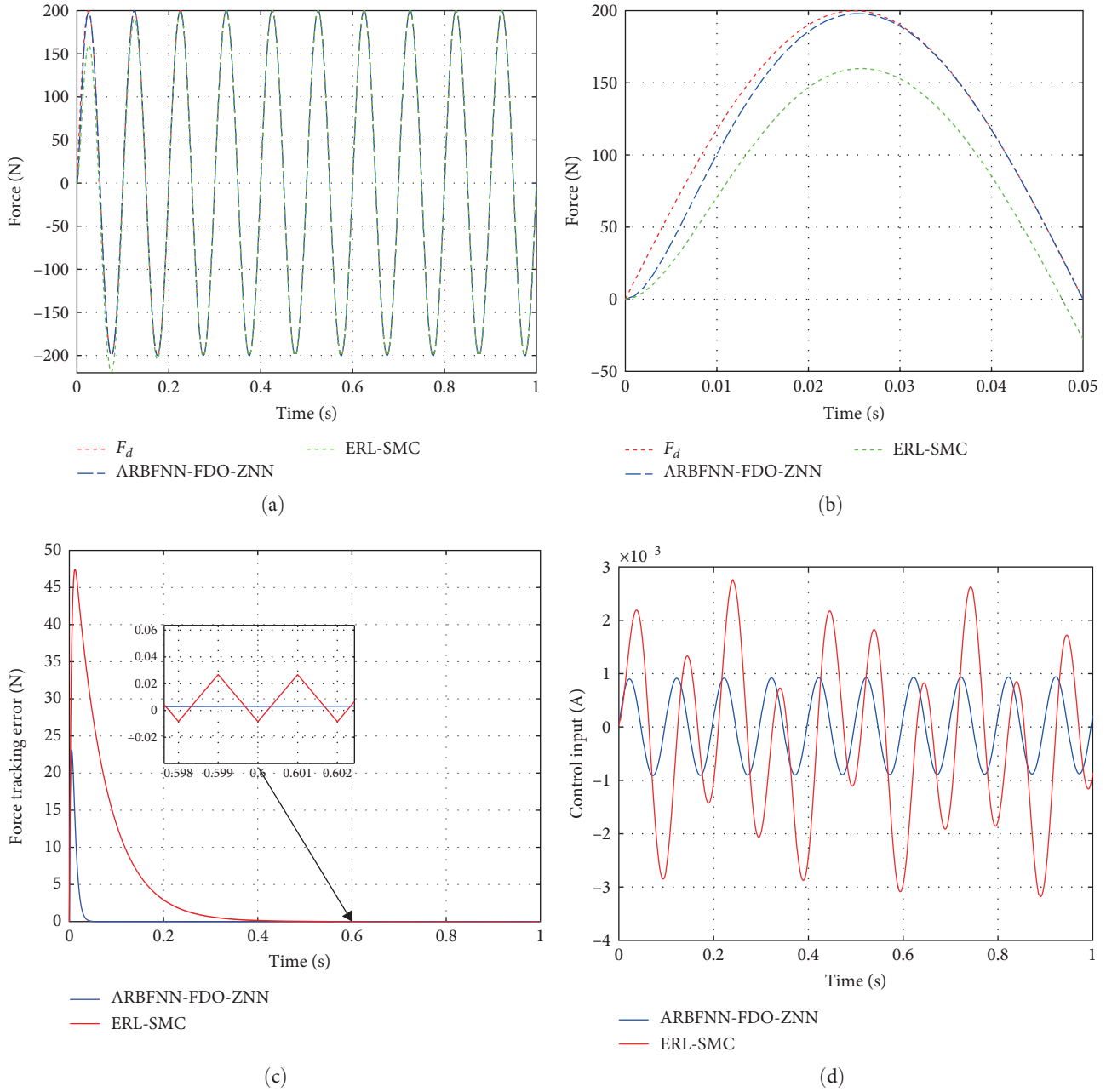

Figure 7: The simulation comparison results with $F_d = 200\sin(20\pi t)$, $\gamma = 200$, and $k = 200$. (a) Represents the overall simulation results, (b) represents the partial enlargement of (a), (c) is the tracking error, and (d) reveals the control input signal.

Table 3: The comparison results with $F_d = 200\sin(4\pi t)$.

Controller	ARBFNN-FDO-ZNN		ERL-SMC	
	$\gamma = 100$	$\gamma = 200$	$k = 100$	$k = 200$
Maximum tracking error	9.24 N	4.62 N	11.41 N	7.58 N
Convergence time	0.113 s	0.047 s	0.403 s	0.385 s

Table 4: The comparison results with $F_d = 200\sin(20\pi t)$.

Controller	ARBFNN-FDO-ZNN		ERL-SMC	
	$\gamma = 200$	$\gamma = 300$	$k = 200$	$k = 300$
Maximum tracking error	23.14 N	15.4 N	47.45 N	33.58 N
Convergence time	0.054 s	0.037 s	0.436 s	0.389 s

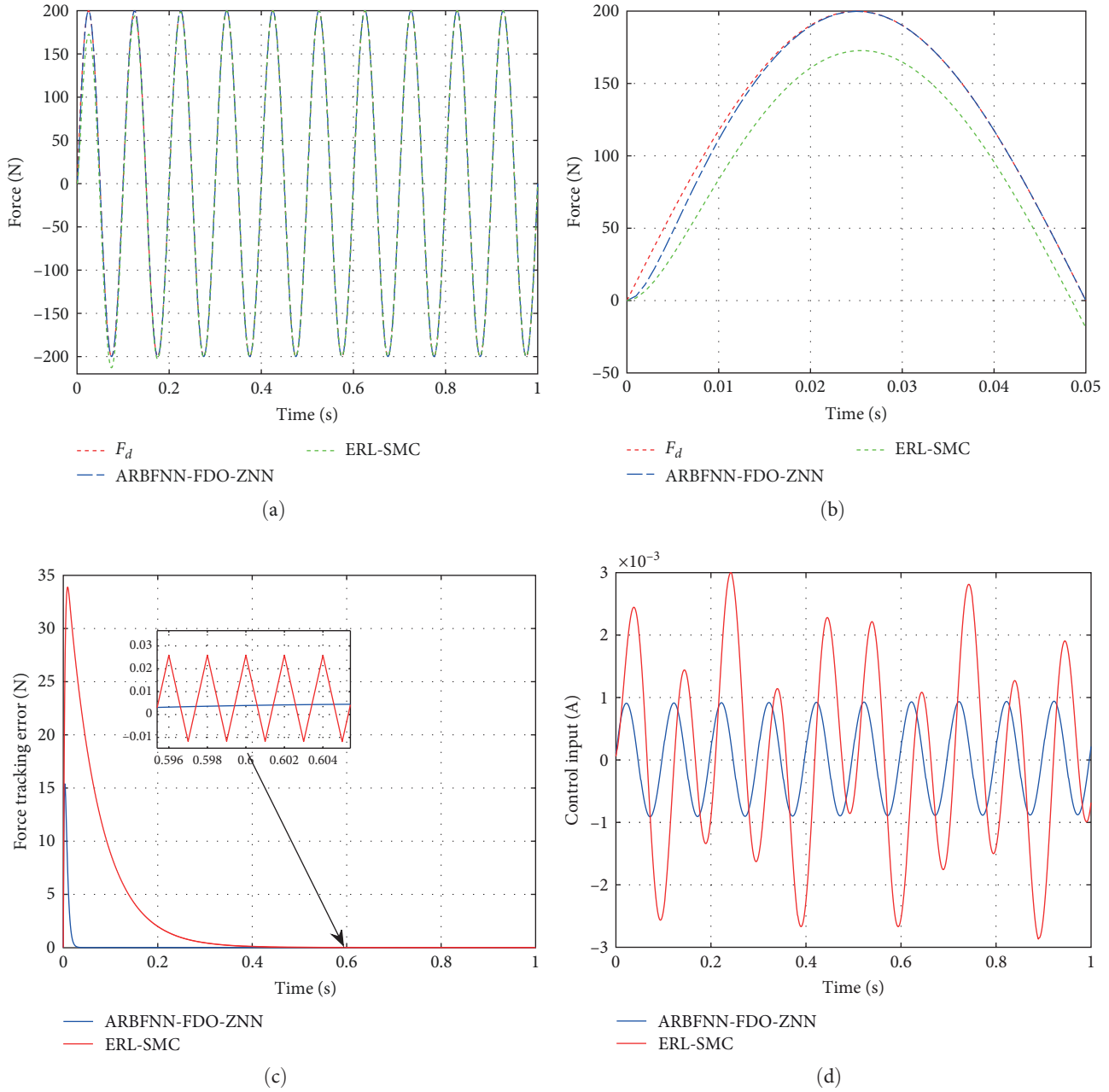

FIGURE 8: The simulation comparison results with $F_d = 200\sin(20\pi t)$, $\gamma = 300$, and $k = 300$. (a) Represents the overall simulation results, (b) represents the partial enlargement of (a), (c) is the tracking error, and (d) reveals the control input signal.

to 300. The result is presented in Figure 14. The maximum tracking error decreases from 25.54 to 16.82 N, a decrease of 34.14%.

Figures 11–14 demonstrate that the tracking error does not strictly converge to 0. First, the theoretical analysis indicates the tracking error converge to 0 with infinite time. Besides, the friction model established in this paper based on the existing friction theory is still different from the practical. Furthermore, due to the uncertainty and disturbance of the system parameters, although the nominal values have been given or estimated in the paper, the changes in the parameters are still unavoidable. Finally, some minor factors such as signal noise affect the performance of the system. Therefore, the actual tracking error and the theoretical differences, a normal phenomenon actually.

Generally, the experimental results indicate the effectiveness of the proposed framework.

6. Conclusions

In this paper, the ARBFNN-FDO-ZNN control scheme has been proposed for the accurate force tracking control of the exoskeleton. Primarily, the ARBFNN is introduced to solve the model uncertainty in the ZNN framework. Then, the FDO is adopted to handle the compound disturbance. The asymptotic stability of the coupled dynamics while applying the

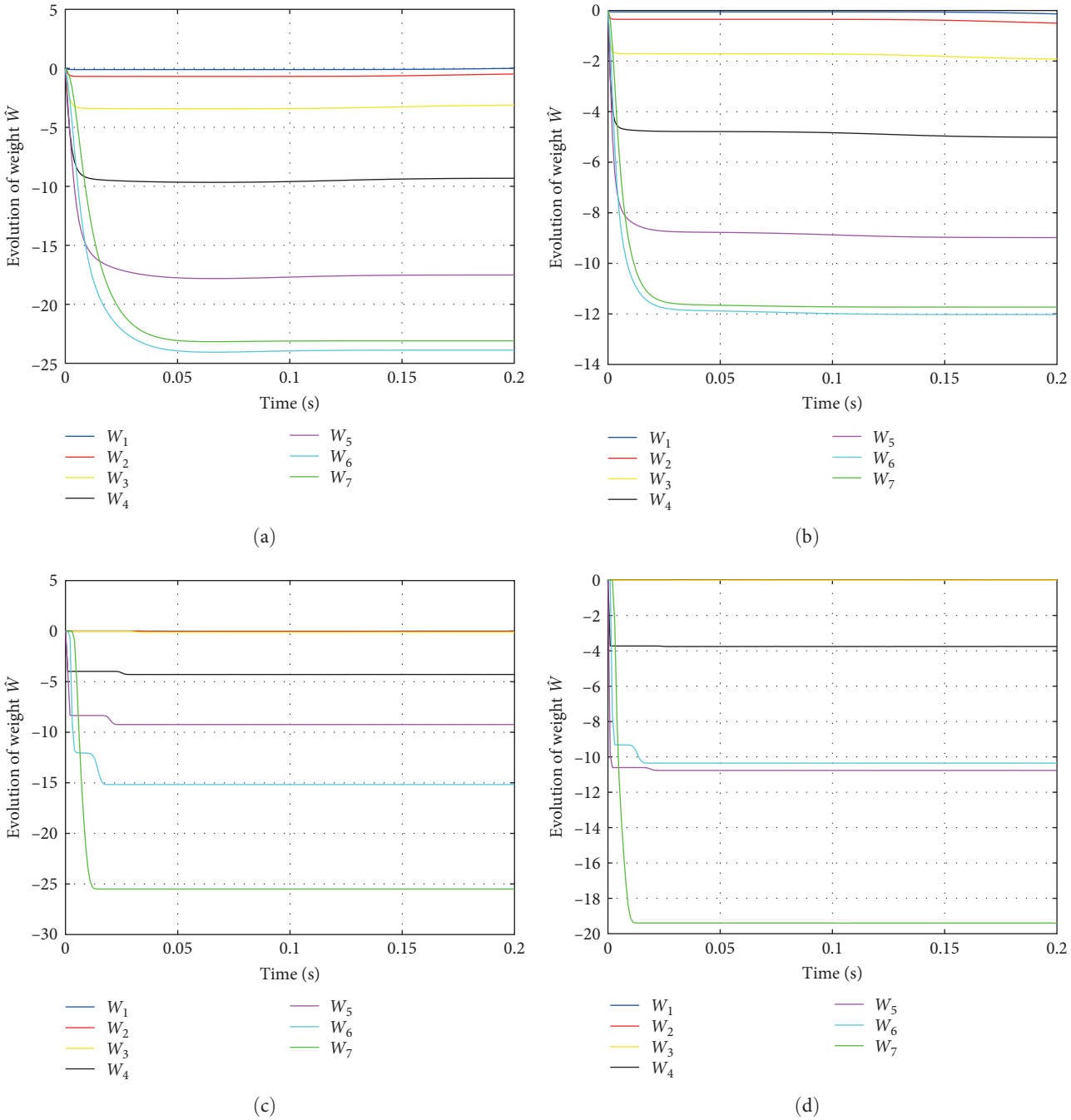

FIGURE 9: Various learning trajectories of the adaptation weights by ARBFNN (a) $F_d = 200\sin(4\pi t)$ and $\gamma = 100$; (b) $F_d = 200\sin(4\pi t)$ and $\gamma = 200$; (c) $F_d = 200\sin(20\pi t)$ and $\gamma = 200$; (d) $F_d = 200\sin(20\pi t)$ and $\gamma = 300$..

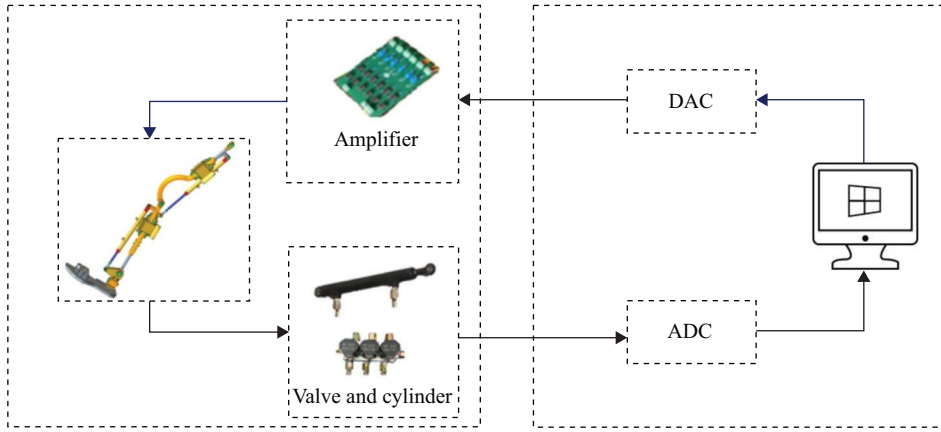

Figure 10: Block diagram of servo system for force tracking control.

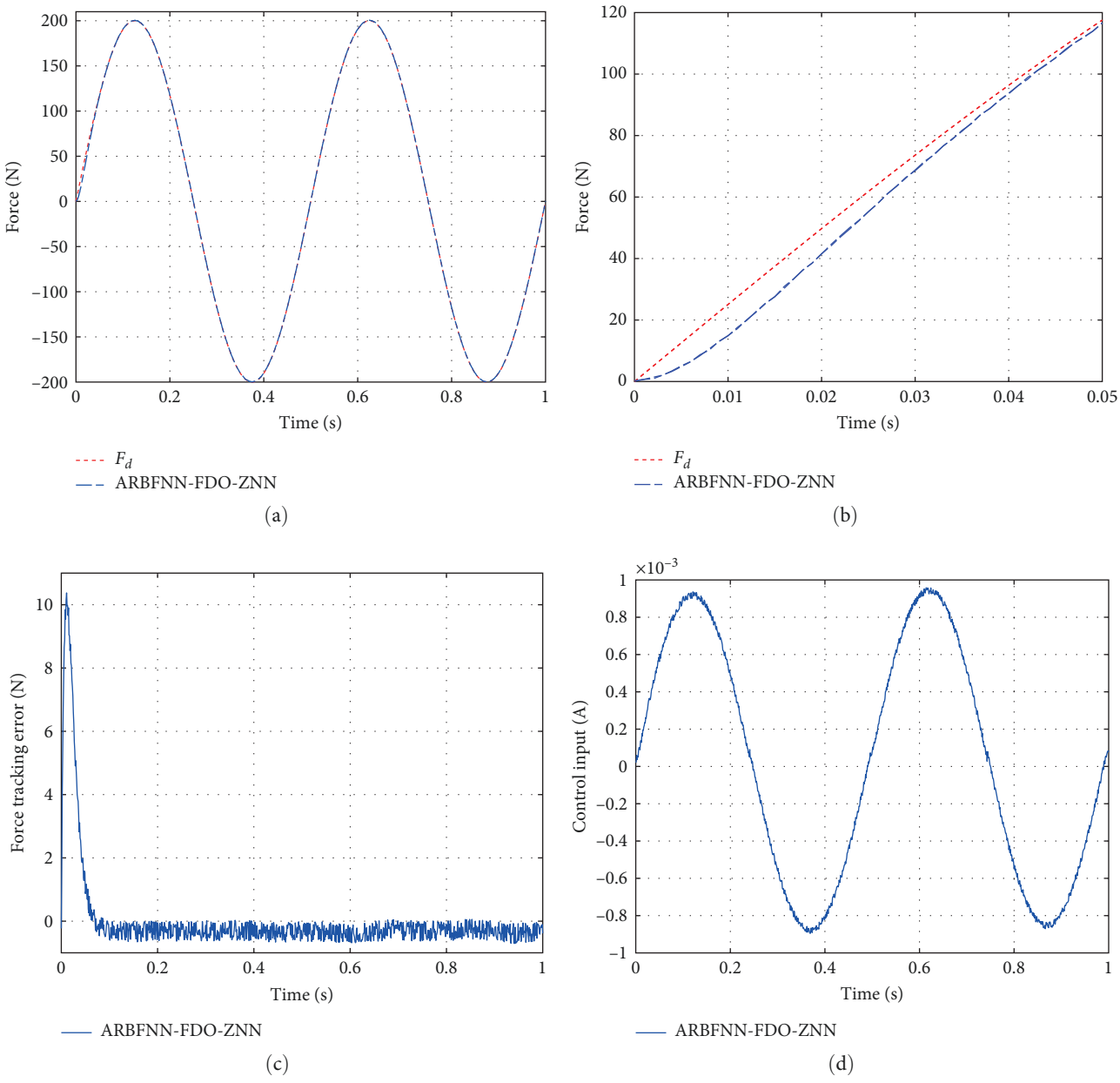

Figure 11: The experimental results with $F_d = 200\sin(4\pi t)$ and $\gamma = 100$. (a) Represents the overall simulation results, (b) represents the partial enlargement of (a), (c) is the tracking error, and (d) reveals the control input signal.

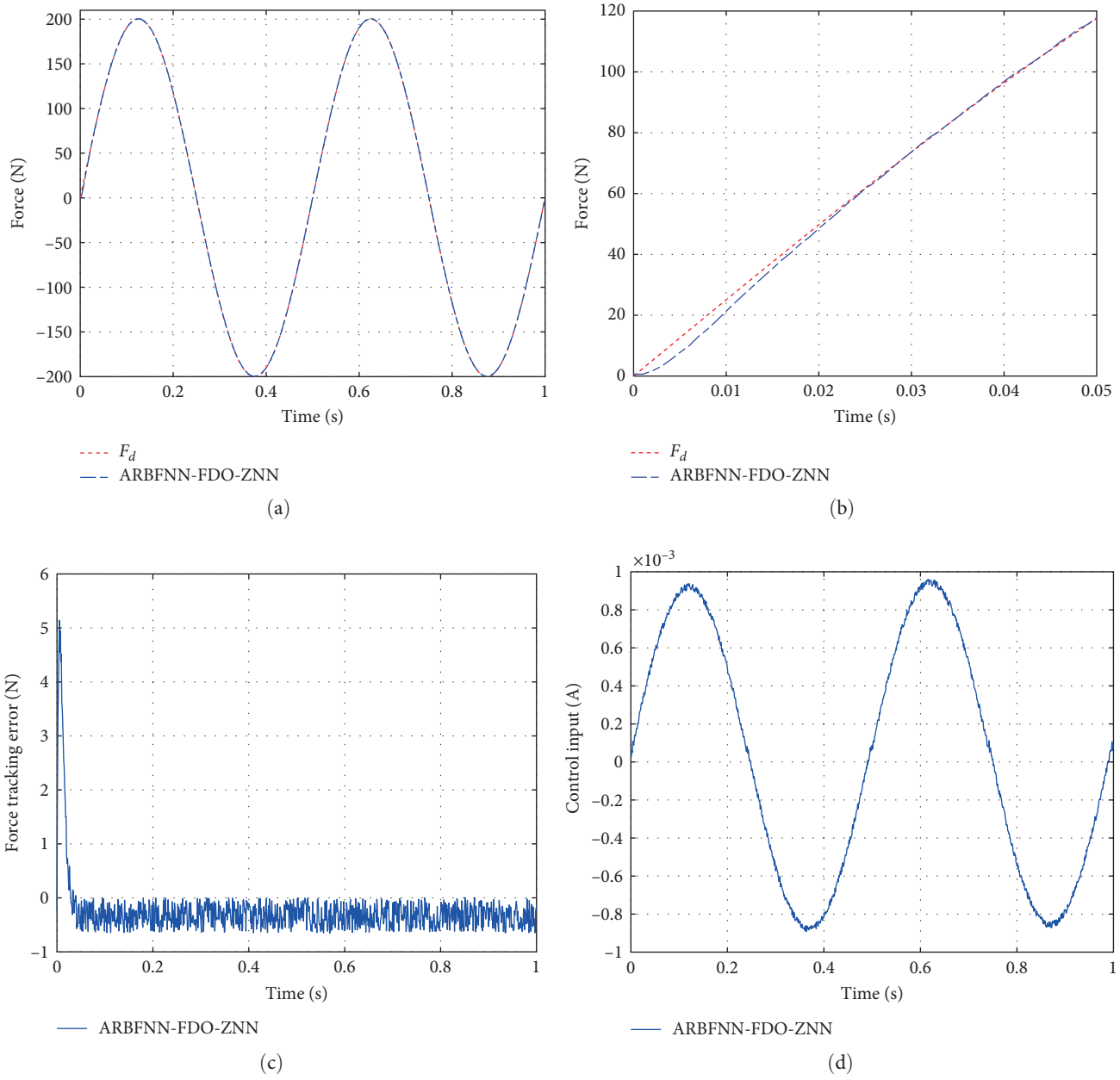

FIGURE 12: The experimental results with $F_d = 200\sin(4\pi t)$ and $\gamma = 200$. (a) Represents the overall simulation results, (b) represents the partial enlargement of (a), (c) is the tracking error, and (d) reveals the control input signal.

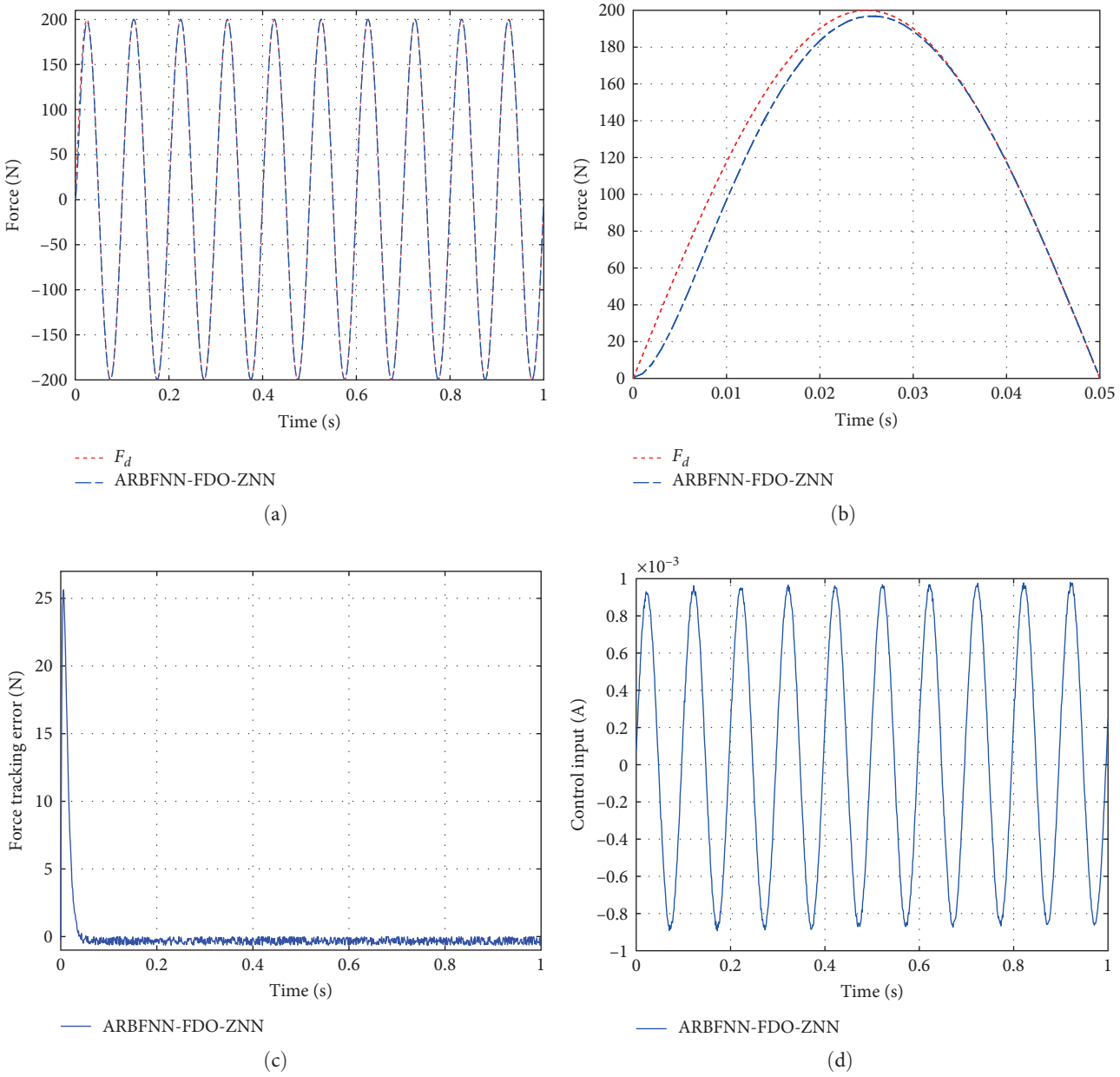

FIGURE 13: The experimental results with $F_d = 200\sin(20\pi t)$ and $\gamma = 200$. (a) Represents the overall simulation results, (b) represents the partial enlargement of (a), (c) is the tracking error, and (d) reveals the control input signal.

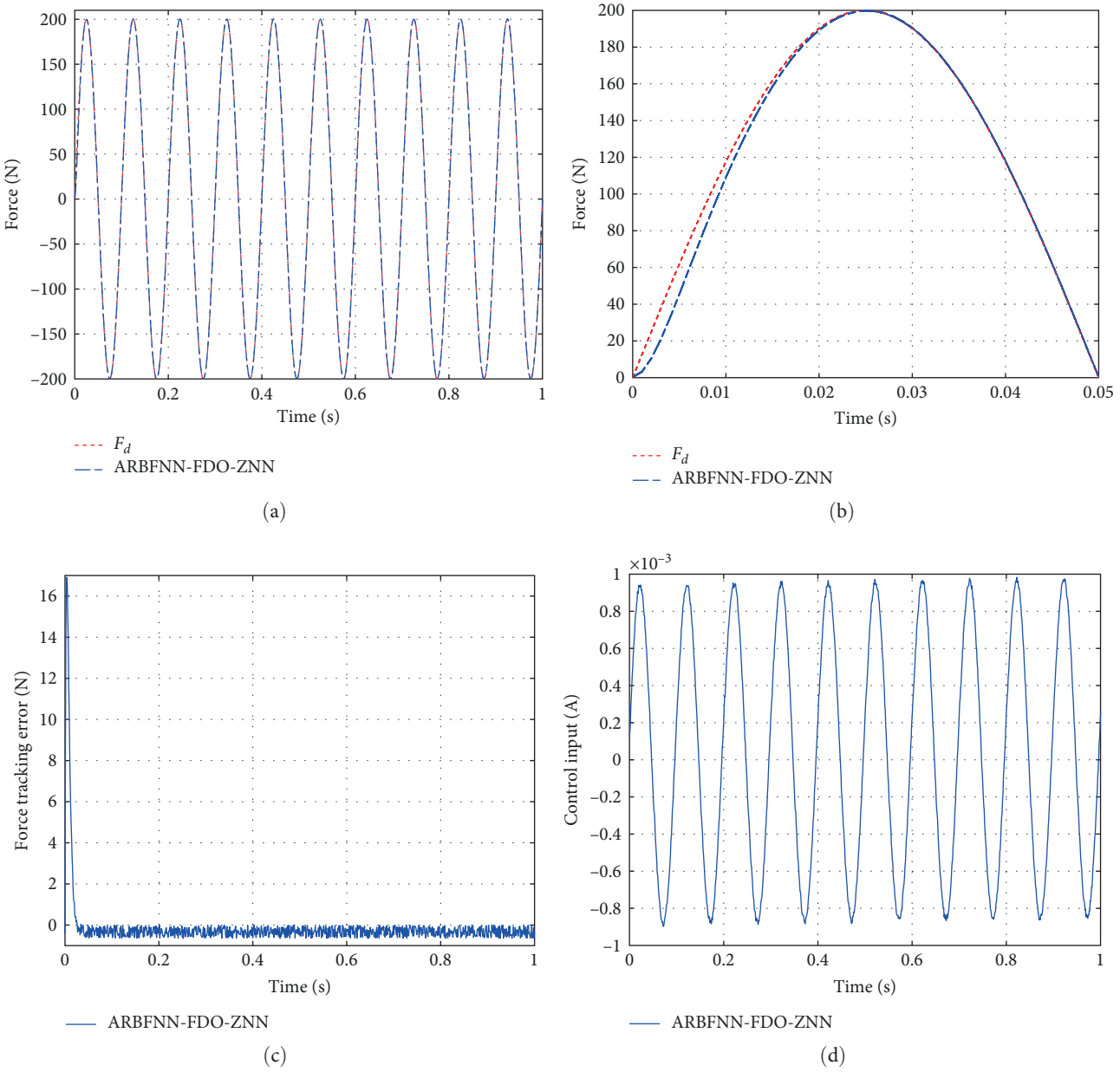

FIGURE 14: The experimental results with $F_d = 200\sin(20\pi t)$ and $\gamma = 300$. (a) Represents the overall simulation results, (b) represents the partial enlargement of (a), (c) is the tracking error, and (d) reveals the control input signal.

proposed control has been ensured using the Lyapunov theory. Compared with ERL-SMC, the simulation results present the superiority of the proposed scheme. Finally, the experimental results have been conducted to present the effectiveness of the scheme.

We incorporated ZNN with observer and RBFNN for the first time. From simulation and experimental results, it has been presented that the proposed approach is effective in fulfilling the force control objective in presence of model uncertainties, external disturbances, and human–robot interaction force. Future work will focus on the extension to the approach to switched control of the lower extremity exoskeleton.

Nomenclature

φ: Joint angle
x_c: Piston displacement
J: System inertia
τ: Mechanical time constant of the spool
M: Moment arm
k_s: DC gain of the valve
F_L: Load force
u: Control variable
F_f: Friction force
A_1, A_2: Areas of piston corresponding to A and B

m: Mass
p_A, p_B: Pressure of chamber A and B
r_o: Mass center
C_{in}, C_{ec}: Hydraulic internal and external leakage of the system
x_v: Spool displacement
V_0: Initial volume of cylinder
μ: Viscous friction coefficient.

Data Availability

The data used to support the findings of this study have not been made available because no new data were created or analyzed in this study.

Conflicts of Interest

The authors declare that they have no conflict of interest.

Acknowledgments

This work has been supported by the Basic Frontier Science and Technology Innovation Project with Army Engineering University KYGYJQZL2210.

References

[1] J. Kang, Z. Wang, H. Cheng, J. Wang, and X. Liu, "Remote sensing land use evolution in earthquake-stricken regions of wenchuan county, china," *Sustainability*, vol. 14, no. 15, Article ID 9721, 2022.

[2] T. Zhang and D. J. Braun, "Theory of fast walking with human-driven load-carrying robot exoskeletons," *IEEE Transactions on Neural Systems and Rehabilitation Engineering*, vol. 30, pp. 1971–1981, 2022.

[3] J. K. Proud, D. T. H. Lai, K. L. Mudie et al., "Exoskeleton application to military manual handling tasks," *Human Factors*, vol. 64, no. 3, pp. 527–554, 2022.

[4] J. Narayan and S. K. Dwivedy, "Robust LQR-based neural-fuzzy tracking control for a lower limb exoskeleton system with parametric uncertainties and external disturbances," *Applied Bionics and Biomechanics*, vol. 2021, Article ID 5573041, 20 pages, 2021.

[5] Y. Yang, X.-C. Dong, Z.-Q. Wu, X. Liu, and D.-Q. Huang, "Disturbance- observer-based neural sliding mode repetitive learning control of hydraulic rehabilitation exoskeleton knee joint with input saturation," *International Journal of Control, Automation and Systems*, vol. 20, no. 12, pp. 4026–4036, 2022.

[6] B. Eshetu and S. Seid, "Modeling and design of ANFIS dynamic sliding mode controller for a knee orthosis of hemiplegia," *Applied Bionics and Biomechanics*, vol. 2023, Article ID 9953957, 17 pages, 2023.

[7] S. Chen, T. Han, F. Dong et al., "Precision interaction force control of an underactuated hydraulic stance leg exoskeleton considering the constraint from the wearer," *Machines*, vol. 9, no. 5, p. 96, 2021.

[8] Y. Yang, X. Dong, X. Liu, and D. Huang, "Robust repetitive learning-based trajectory tracking control for a leg exoskeleton driven by hybrid hydraulic system," *IEEE Access*, vol. 8, pp. 27705–27714, 2020.

[9] S. Lee, P. Y. Li, and F. Eskilsson, "Energetically passive multi-degree-of-freedom hydraulic human power amplifier with assistive dynamics," *IEEE Transactions on Control Systems Technology*, vol. 28, pp. 1296–1308, 2020.

[10] Z. Gan, H. Tang, E. Treadway, R. B. Gillespie, and C. D. Remy, "Modeling and experimental evaluation of a variable hydraulic transmission," *IEEE/ASME Transactions on Mechatronics*, vol. 25, pp. 750–761, 2020.

[11] Y. Han, S. Liu, J. Chang et al., "Design and preliminary evaluation of a lower limb exoskeleton based on hydraulic actuator," *Industrial Robot: the International Journal of Robotics Research and Application*, 2023.

[12] X. Zhang, W. Jiang, Z. Li, and S. Song, "A hierarchical Lyapunov-based cascade adaptive control scheme for lower-limb exoskeleton," *European Journal of Control*, vol. 50, pp. 198–208, 2019.

[13] L. Lang, J. Xiao, Y. Sun, H. Lu, Z. Zhou, and C. Yang, "Scale force control of an exoskeleton for human performance augmentation," *Journal of Intelligent & Robotic Systems*, vol. 106, no. 1, Article ID 22, 2022.

[14] L. Cheng, Z.-C. Zhu, G. Shen, S. Wang, X. Li, and Y. Tang, "Real-time force tracking control of an electro-hydraulic system using a novel robust adaptive sliding mode controller," *IEEE Access*, vol. 8, pp. 13315–13328, 2020.

[15] S. Chen, H. Zhang, T. Han, F. Dong, H. Liu, and J. Han, "Adaptive robust force control of an underactuated walking lower limb hydraulic exoskeleton," *Transactions of the Institute of Measurement and Control*, vol. 45, no. 5, pp. 940–954, 2023.

[16] S. Song, Y. Cao, H. Wang et al., "Adaptive output feedback force tracking control for lower extremity power assisted exoskeleton," *Control Engineering and Applied Informatics*, vol. 20, pp. 60–68, 2018.

[17] Y. Zhang and J. Wang, "Recurrent neural networks for nonlinear output regulation," *Automatica*, vol. 37, no. 8, pp. 1161–1173, 2001.

[18] Y. Zhang, D. Jiang, and J. Wang, "A recurrent neural network for solving Sylvester equation with time-varying coefficients," *IEEE Transactions on Neural Networks*, vol. 13, no. 5, pp. 1053–1063, 2002.

[19] W. Li, X. Ma, J. Luo, and L. Jin, "A strictly predefined-time convergent neural solution to equality- and inequality-constrained time-variant quadratic programming," *IEEE Transactions on Systems, Man, and Cybernetics: Systems*, vol. 51, no. 7, pp. 4028–4039, 2021.

[20] Z. Zhang, L. Zheng, T. Qiu, and F. Deng, "Varying-parameter convergent–differential neural solution to time-varying over determined system of linear equations," *IEEE Transactions on Automatic Control*, vol. 65, pp. 874–881, 2020.

[21] L. Zheng and Z. Zhang, "Convergence and robustness analysis of novel adaptive multilayer neural dynamics-based controllers of multirotor UAVs," *IEEE Transactions on Cybernetics*, vol. 51, no. 7, pp. 3710–3723, 2021.

[22] L. Zheng, F. Deng, Z. Yu, Y. Luo, and Z. Zhang, "Multilayer neural dynamics-based adaptive control of multirotor UAVs for tracking time-varying tasks," *IEEE Transactions on Systems, Man, and Cybernetics: Systems*, vol. 52, no. 9, pp. 5889–5900, 2022.

[23] J. Dai, L. Luo, L. Xiao, L. Jia, and X. Li, "An intelligent fuzzy robustness ZNN model with fixed-time convergence for time-variant Stein matrix equation," *International Journal of Intelligent Systems*, vol. 37, no. 12, pp. 11670–11691, 2022.

[24] Z. Li, B. Huang, Z. Ye, M. Deng, and C. Yang, "Physical human–robot interaction of a robotic exoskeleton by

admittance control," *IEEE Transactions on Industrial Electronics*, vol. 65, pp. 9614–9624, 2018.

[25] D. Zhang, L. Kong, S. Zhang, Q. Li, and Q. Fu, "Neural networks-based fixed-time control for a robot with uncertainties and input deadzone," *Neurocomputing*, vol. 390, pp. 139–147, 2020.

[26] W. He, Y. Sun, Z. Yan, C. Yang, Z. Li, and O. Kaynak, "Disturbance observer-based neural network control of cooperative multiple manipula-tors with input saturation," *IEEE Transactions on Neural Networks and Learning Systems*, vol. 31, pp. 1735–1746, 2020.

[27] X. Yao, J. H. Park, L. Wu, and L. Guo, "Disturbance-observer-based composite hierarchical antidisturbance control for singular markovian jump systems," *IEEE Transactions on Automatic Control*, vol. 64, pp. 2875–2882, 2019.

[28] Y. Yang, Y. Li, X. Liu, and D. Huang, "Adaptive neural network control for a hydraulic knee exoskeleton with valve deadband and output constraint based on nonlinear disturbance observer," *Neurocomputing*, vol. 473, pp. 14–23, 2022.

[29] S. S. Ge and C. Wang, "Adaptive neural control of uncertain MIMO nonlinear systems," *IEEE Transactions on Neural Networks*, vol. 15, no. 3, pp. 674–692, 2004.

[30] T. Yang, X. Yi, J. Wu et al., "A survey of distributed optimization," *Annual Reviews in Control*, vol. 47, pp. 278–305, 2019.

[31] L. Zhao, J. Jin, and J. Gong, "Robust zeroing neural network for fixed-time kinematic control of wheeled mobile robot in noise-polluted environment," *Mathematics and Computers in Simulation*, vol. 185, pp. 289–307, 2021.

[32] L. Zheng and Z. Zhang, "Time-varying quadratic-programming-based error redefinition neural network control and its application to mobile redundant manipulators," *IEEE Transactions on Automatic Control*, vol. 67, no. 11, pp. 6151–6158, 2022.

[33] S. Song, X. Zhang, and Z. Tan, "RBF neural network based sliding mode control of a lower limb exoskeleton suit," *Strojniški vestnik – Journal of Mechanical Engineering*, vol. 60, no. 6, pp. 437–446, 2014.